OPEN ACCESS PLATINUM
CC BY NC ND

Contributions to Geophysics and Geodesy Vol. 54/3, 2024 (279–300)

The structural elements controlling the subsurface mineralization as deduced from the integration of magnetic and self-potential methods, Wadi Khosh El-Daba area, southern Sinai, Egypt

Mohamed H. M. YOUSEF*

Nuclear Materials Authority, P.O. Box, 530, Maadi, Cairo, Egypt

Abstract: Significant copper mineralization are observed to be associated, in most cases, with some radioactive anomalies related to increased uranium and thorium contents in Southern Sinai, Egypt. These mineralizations are related to intense post-magmatic, structurally controlled hydrothermal activities in many localities. Wadi Khosh El-Daba area is one of these locations which is mainly composed of monzogranites dissected by andesite dyke and pegmatite vein. This work deals with the application of ground magnetic and self-potential methods to establish the magnetic sources governing the mineralization, to interpret the significant trends that affected the study area, and to delineate the mineralized zones. The magnetic data were processed, enhanced and interpreted using advanced techniques, such as the first-order vertical derivative (FVD), the tilt derivative (TD), Euler deconvolution (ED), and source parameter image (SPI). The main structural lineaments/contacts that control the distribution of hydrothermal alterations and mineral distributions are oriented to the NW–SE, NE–SW, and NNW–SSE directions. The self-potential (SP) data show that there are numerous mineralized zones; most of them are distributed mainly along the structural lineaments deduced from the magnetic study. The quantitative interpretation revealed that the mineralized bodies are at shallow depths ranging from 5.6 m to 12.7 m, with half-width from 5 m to 13 m. These bodies are shallow to moderate dipping towards the south and north directions. Based on this study an anomaly map is originated to locate the preferred structural elements that may be controlling the mineralization in the area for further future exploration.

Key words: ground magnetic, self-potential, southern Sinai, Egypt

1. Introduction

The southern part of Sinai, some 20,000 km^2 in area, is mainly covered by different varieties of the basement rocks which dominated by granites about 70% (*Bentor, 1985*) of Precambrian ages. Some of the granite rocks are asso-

*corresponding author, e-mail: mhm_sinai@yahoo.com

doi: 10.31577/congeo.2024.54.3.4

ciated with different mineralized occurrences of economic importance such as copper (e.g., *El Shazly, 1959; Gindy, 1966; Bogoch and Zilberfrab, 1979; Hassen, 1987* and *El-Ghawaby et al., 2000*), sulphide (e.g., *El-Ghawaby, 1984* and *Hassen, 1987*) and uranium (e.g., *Ibrahim, 1991; Bishr, 2007* and *Mousa et al., 2014*).

Wadi Khosh El-Daba area, which is the subject of this study, is one of the tributaries of Wadi El-Regeita area which is situated in the central part of southern Sinai (Fig. 1). It is located at the intersection of latitude 28° 37′ 44″ N and longitude 34° 4′ 43” E. The area is characterized by a low to moderate topographic relief and exposed outcrops which facilitate studying the geological setting.

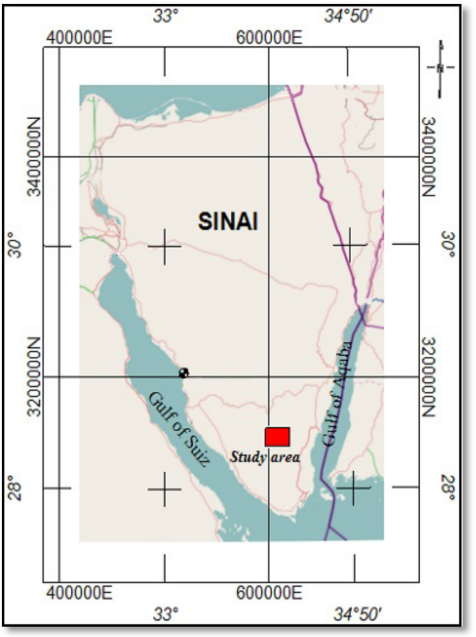

Fig. 1. Location map of Wadi Khosh El-Daba area, Southern Sinai, Egypt.

This area acquired its importance after the discovery of radioactive anomalies related to uranium mineralization (*Bishr and Moselhy, 2008*). For this reason, Wadi Khosh El-Daba area was selected for this geophysical study, on the basis of uranium occurrences. The objectives of the present study are: 1) the use of a ground magnetic survey to establish the magnetic sources

governing the mineralization, and interpret the significant trends that affected the study area; 2) to follow the anomalous surface mineralization at deeper depths and obtain information about their lateral and vertical extensions through application of the self-potential (SP) survey method.

2. Geological background and mineralization

The study area is composed mainly of the monzogranite rock dissected by post-granitic andesite dyke and pegmatite vein (Fig. 2). The monzogranite is pale pink in colour, medium to coarse-grained and highly jointed with predominant NE–SW, NNW–SSE, and NW–SE trends. Based on the petrochemical investigations, *Niazy et al. (1995)* classified the younger granite as Perthitic leucogranite of calc-alkaline magma series. It is also considered as two-feldspar younger granite, similar to G-2 granites of *Hussein et al. (1982)*. Structurally, the exposed younger granite is highly affected by fundamental NE–SW fractures as a result of the major faulting parallel to the Gulf of Aqaba (*El-Gammal, 1986*).

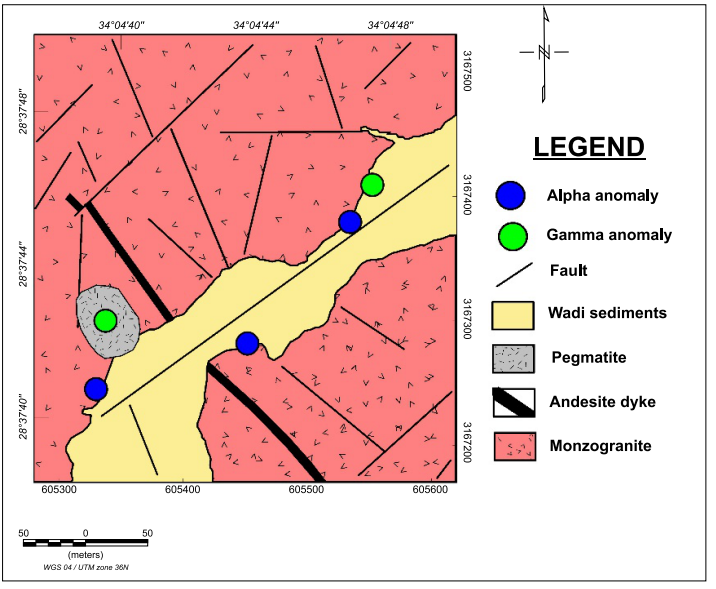

Fig. 2. Geological map of Wadi Khosh El-Daba area showing the locations of the alpha and gamma anomaly, Southern Sinai, Egypt (*Bishr and Moselhy, 2008*).

Regarding to the post-granitic dykes, they are dominated by the andesite rocks, extruded along the fractures and faults in the NW–SE direction. The rocks are black or very dark grey in colour and fine-grained with porphyritic texture. Some of the andesite dykes are associated with Cu mineralization, and show abundant disseminations of hematite, which is mostly associating the effect of epigenetic Cu-mineralizing solutions. Finally, the post-granitic pegmatite vein is associated with fault planes occupying ENE–WSW and NNE–SSW directions. Pegmatite is very coarse-grained and composed of quartz, alkali feldspar and plagioclase. Some parts of the pegmatite vein bear green copper staining.

Hassen (1987) revealed that the copper mineralization in El-Regeita area is lithologically and structurally controlled and the copper mineralization accompanies fault planes of 65°N – 70°W strike trends. *Ibrahim (1991)* identified two deformation trends (ENE–WSW and N–S) in Wadi Zaghra area to the east of the present study area. He defined two episodes for the formation of thorium (Th) and uranium (U) mineralizations along these deformation trends associated with secondary copper mineralization carried by hydrothermal solutions. *El-Assey et al. (1994)* through their study in Um Alawi environs, which include the present study area, found that the enrichment of uranium and thorium was found to be mostly structurally controlled. The intensity of radioactivity and associated alterations increase at the intersection of the NW fault zones with the NE faults. They proposed that the later hydrothermal solutions enriched in uranium led to the alteration of the host rocks and the formation of the uranium-thorium minerals. The hydrothermal solutions also affected the pegmatite pockets which were enriched in uranium. *El-Ghawaby et al. (2000)* concluded that the hydrothermal mineralization of Saint Katherine area has been ejected during the late stage of the intrusion of the granitic magma. The spatial distribution of the copper mineralization shows a close relation with alteration, faults and dykes. *Bishr (2007)* through his study in Wadi El-Regeita area, including Wadi Khosh El-Daba, indicates that radiometric anomalies are generally associated with highly altered spots due to secondary U minerals. The hydrothermal fluids are responsible for the observed uranium mineralization that has been transported from deeper sources through the structural weakness of the shear zones.

In the present study area, *Bishr and Moselhy (2008)* used alpha particle

tracks in their study to detect the radon as a guide for subsurface uranium occurrences. They discovered surface mineralization associated with pegmatite body and four subsurface anomalies. They believed that these anomalies are associated with the down-faulted. The study indicates the presence of uranium minerals in fissure planes that are tectonically controlled. They suggest the increase of radioactive minerals in-depth and hydrothermal solution are responsible for uranium and thorium-bearing minerals. Therefore, they considered the area valuable for radioactive mineralization connected with the subsurface of fracture. They suggest further work to follow up on the form and setting of the uranium mineralization in the subsurface zone (*Bishr and Moselhy, 2008*).

3. Geophysical field survey

3.1. Ground magnetic survey

The purpose of magnetic surveying is to identify and describe regions of the Earth's crust that have unusual (anomalous) magnetizations. In the realm of applied geophysics the anomalous magnetizations might be associated with local mineralization that is potentially of commercial interest (*Lowrie, 2007*).

In the present study, a systematic ground magnetic survey has been carried out for an area of 360 × 340 m, on a grid pattern of 20 m station separation through 18 N–S parallel profiles of 360 m length for each. The total-intensity of magnetic field measurements were performed using a portable proton-precession magnetometer, model PMG-1, Geofyzika Brno, Czech Republic, having a sensitivity of 0.1 nT and a measuring range from 25,000 to 100,000 nT.

3.2. Self-potential (SP) survey

The self-potential (SP) method is based upon the natural potential difference between any two points in the ground. These potentials, which are mainly constant although they vary irregularly at times, are associated with electric currents within the ground. With the self-potential method, the distribution of the electrical potential at the surface of the Earth (or in boreholes) is measured with respect to a reference electrode ideally placed at

infinity (e.g. *Sato and Mooney, 1960*). These potentials are set up by electrochemical reactions in the subsurface rocks and/or in the bodies which may occur within these rocks and can be separated into two basic categories. Firstly, there are small background potentials which can be either positive or negative which lie within the range of a fraction of a millivolt to a few millivolts. Secondly, there are large mineralization potentials which may go to hundreds of millivolts and are typically negative (*Telford et al., 1990*).

This method evidences polarization processes occurring at depth. For example, the occurrence of strong negative self-potential anomalies associated with the presence of ore deposits has been known since the nineteenth century (e.g. *Fox 1830; Bølviken and Logn 1975; Church, 1984; Elkattan et al., 1996; Bigalke et al., 2004; Sultan et al., 2009; Mousa et al., 2014; Assran et al., 2018, Horo et al., 2023*). The amplitude of these anomalies usually reaches a few hundred millivolts. *Goldie (2002)* reported a self-potential anomaly amounting to −10.2 V associated with the high sulphide gold deposit. Negative self-potential signals of several hundred mV have also been observed in association with contaminant plumes, rich in organic matter, associated with leakage from municipal landfills (*Nyquist and Corry, 2002; Arora et al. 2007*).

As the method offers relatively rapid field data acquisition, it often is cost-effective for reconnaissance or initial investigation of an area prior to more intensive studies using other geophysical and geochemical techniques (*Telford et al., 1990; Parasins, 1997*).

SP's are difficult to observe through high resistivity surface rocks, therefore, a high impedance voltmeter instrument is used. Accordingly, the meter used in the present work is an auto-ranging digital multimeter model HP 972A (U.S.A. made), along with two non-polarizing electrodes. These non-polarizing electrodes are usually made of porous pots containing a saturated solution of copper sulphate. The fixed electrode technique was chosen to conduct the SP survey in the present study area. In this approach, one electrode is fixed at the selected base station and the other is moving along the profile. The electrodes are placed in 10 cm holes, which made at each station on a grid pattern, to reduce the source of noise from the topsoil. Watering of these holes may improve contact consistency (*Semenov, 1974*). All the individual base stations (base for each profile) were reduced relative

to the zero value of the selected general base station. Figure 10a illustrates the location of the selected area for conducting the SP survey. The sample interval of observation along the profiles was 20 m and the distance between the profiles was 40 m. The length of each profile is 360 m. After the reduction of the SP data, the value of the base station of each profile was subtracted or added to the value of each station along the same profile. The reduced values were plotted and contoured in map form (Fig. 10b).

4. Data processing and interpretation

4.1. Ground magnetic data

The corrections which are performed to the ground magnetic data included the correction for the diurnal variations, normal-field which is required to take into account the normal variation of the geomagnetic field intensity with latitude and longitude (*Sharma, 1997*), and tie line correction.

There are no comments regarding the data quality, disturbances or problems during the survey, and no potential post processing is discussed. In Figure 3 the distribution of the magnetic data is presented in a histogram. The distribution is smooth and lognormal, which is normally expected for high quality data. Profile plots and test gridding also indicates natural variations and there are no indications of outliers or physically unreliable anomalies. Hence, the quality of the magnetic dataset appears to be high.

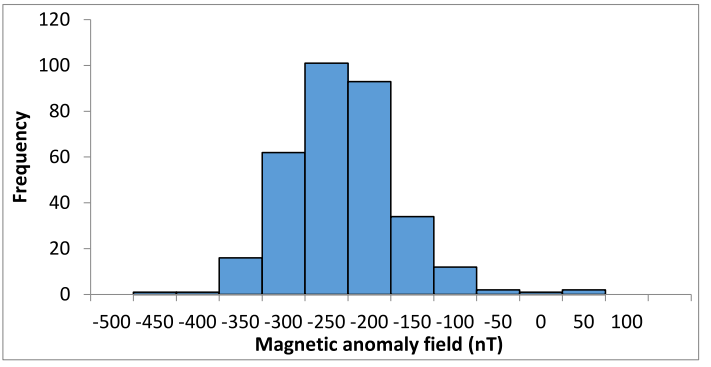

Fig. 3. Histogram showing the distribution of the total magnetic anomaly field data, Wadi Khosh El-Daba area, Southern Sinai, Egypt.

Because of the inclination of the earth's magnetic field, most magnetic anomalies show both positive and negative responses. These minima and maxima are generally offset from the centre of the causative body along the magnetic meridian. Only in the case where the inclination is 90° the magnetic anomaly lies directly over the centre of the source body. The method of reduction to the pole (RTP) is used to remove this effect, so that the data appear as if observed at the pole, where the magnetic field is vertical. The magnetic maxima, then, occur directly over the magnetized bodies (*Kearey and Brooks, 1991*). In the present study, the total intensity magnetic map (Fig. 4a) was reduced to the northern magnetic pole (Fig. 4b), utilizing the known inclination and declination of the study area (I = 42.6°, D = 3.98°).

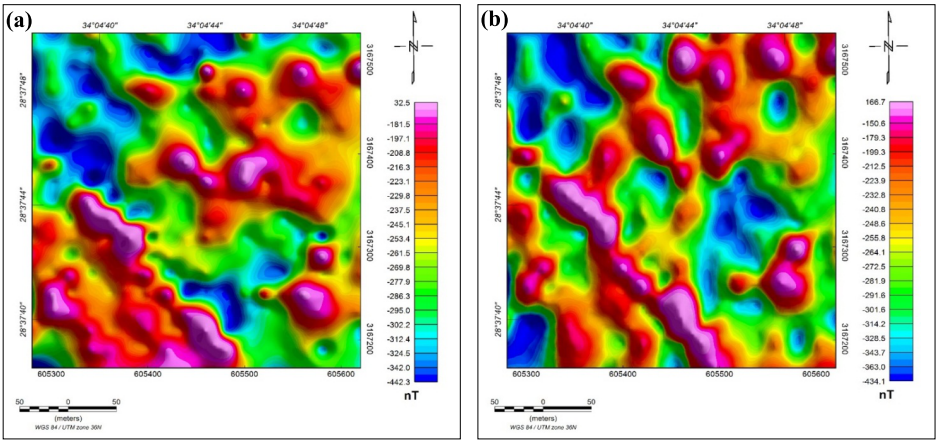

Fig. 4. Shaded-colour map of the total intensity magnetic field (a); the reduced to the north magnetic pole (RTP) component in nT (b), Wadi Khosh El-Daba area, Southern Sinai, Egypt.

Magnetic data observed in geological surveys are the sum of magnetic fields produced by all the underground sources. The targets for specific surveys are often small-scale structures that occur at shallow depths. The magnetic responses of these targets are embedded in a regional field, which arises from magnetic sources usually larger or deeper than these targets. Correct estimation and removal of the regional field from the initial effect yields the residual response produced by the target sources. Therefore, Fast Fourier Transform (FFT) was applied to the RTP magnetic data using *Geosoft (2014)*, to explore the frequency content of these data and to select

the suitable cut-off frequency for carrying out both the high-pass and low-pass filtered maps. As a result of visual inspection of the two-dimensional power spectrum (Fig. 5) two linear segments were distinguished and fitted.

The inspection of the power spectrum curve of the study area reveals that the frequencies of the near-surface magnetic component vary between 10.0 and 43.0 cycle/grid unit, meanwhile the deep-seated magnetic component is distinguished by a frequency band ranging from 2.0 to 8.0 cycle/grid unit (Fig. 5). These bands of frequencies were used to produce the high-pass (residual) and the low-pass (regional) maps (Figs. 6a and 6b) using the band-pass filter technique (*Geosoft, 2014*). The estimated average depths for the shallow and deep magnetic sources as calculated from the power spectrum curve are 19 m and 37 m, respectively. This is consistent with the results of the magnetic study of the Wadi El-Regeita area, adjacent to the current study area (*Yousef, 2014*), since the estimated average depths for the shallow and deep magnetic sources as calculated from the power spectrum for this area were 15 m and 44 m.

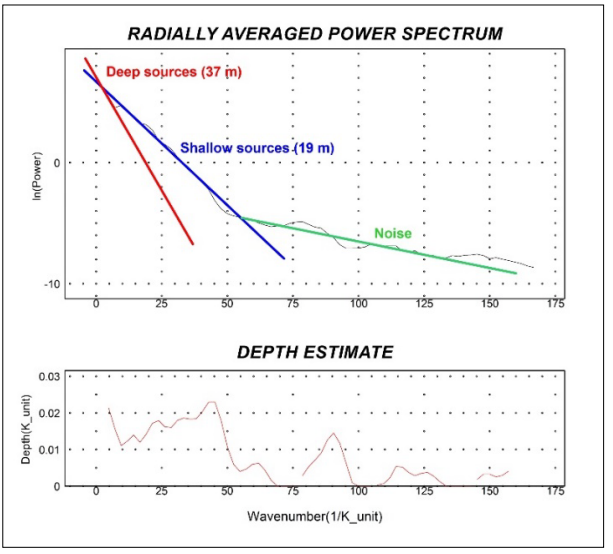

Fig. 5. Average power spectrum curve of the RTP magnetic data, Wadi Khosh El-Daba area, Southern Sinai, Egypt.

The RTP magnetic map was subjected to first-order vertical derivative (FVD), tilt derivative (TDR), Euler deconvolution, and source parameter

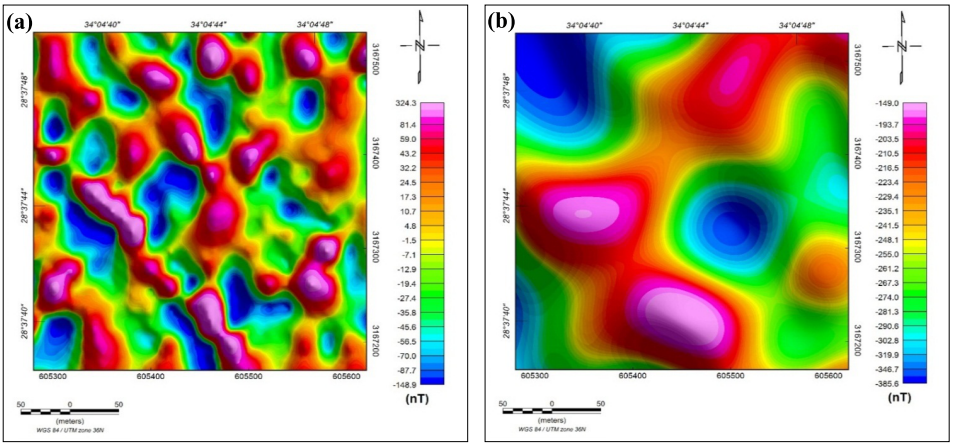

Fig. 6. Shaded-colour map of the residual magnetic component (a); the regional magnetic component in nT (b), Wadi Khosh El-Daba area, Southern Sinai, Egypt.

image (SPI) to highlight and delineate the near-surface lineament structure, such as faults, contacts, dykes, and shear zone, which may play major roles in the distribution of mineral deposits.

To locate near-surface magnetic characteristics connected to geological formations, an FVD map is essential since it is sensitive to magnetic sources close to the surface. The FVD map's zero-contour value facilitates the differentiation of lithological and structural features. Figure 7a illustrates the FVD map of the magnetic data.

The TDR method has been used to map shallow basement formations and find possibilities for mineral prospecting; however, it is useless for this purpose because the edges of deep sources are never detected. According to *Miller and Singh (1994)*, the tilt derivative (TDR) method is expressed as the following:

$$\mathrm{TDR} = \tan^{-1}(\mathrm{VDR}/\mathrm{HGM})\,,$$

where VDR is the vertical derivative of the magnetic field, and HGM is its horizontal gradient magnitude. By applying a threshold of 0.0 and plotting the "zero-contour" it is possible to isolate all bodies with a positive susceptibility contrast. The TDR map of the magnetic data of the study area is presented in Fig. 7b.

Reid et al. (1990) employed gridded data and generalized the Euler de-

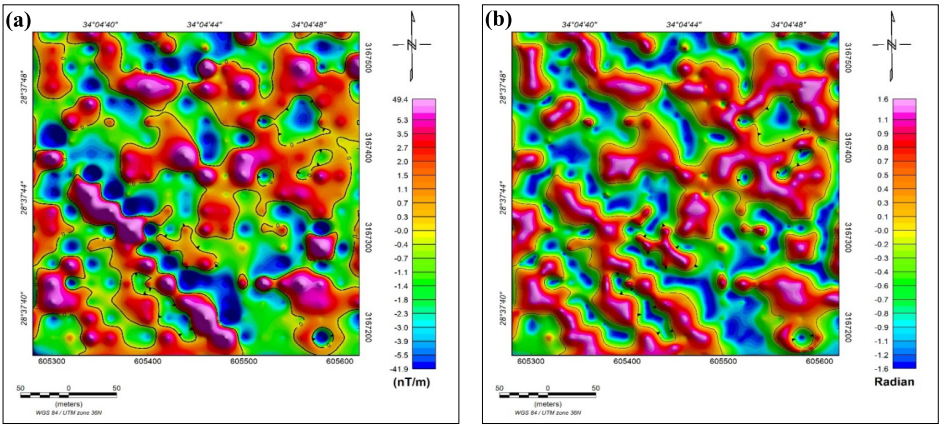

Fig. 7. Shaded-color map of the first-order vertical derivative (FVD) (a); the tilt derivative (TDR) (b), Wadi Khosh El-Daba area, Southern Sinai, Egypt.

convolution to show the position and depth of the magnetic sources. This technique has successfully been utilized in identifying lineaments and geological structures (contacts and faults). *Barbosa et al. (1999)* suggested modifications to Euler deconvolution for application to magnetic data:

$$\frac{\partial T}{\partial x}(x - x_0) + \frac{\partial T}{\partial y}(y - y_0) + \frac{\partial T}{\partial z}(z - z_0) = N(B - T),$$

where T is the total field detected at (x, y, z) by the magnetic source at position (x_0, y_0, z_0), B is the background value of the total field, and N is the degree of homogeneity or geo-physics related to the structural index (SI). The Euler deconvolution solutions map of the study area using SI = 0 (for contacts) is shown in Fig. 8a.

Source Parameter Imaging (SPI) is a technique based on the extension of complex analytic signal to estimate magnetic depths, it is also known as a local wavenumber. The original SPI method (*Thurston and Smith, 1997*) works for two models: a 2-D sloping contact or a 2-D dipping thin-sheet. For the magnetic field M, the local wavenumber (*Thurston and Smith, 1997*) is given by:

$$K = \frac{\dfrac{\partial^2 M}{\partial x \partial z}\dfrac{\partial M}{\partial x} - \dfrac{\partial^2 M}{\partial x^2}\dfrac{\partial M}{\partial z}}{\left(\dfrac{\partial M}{\partial x}\right)^2 + \left(\dfrac{\partial M}{\partial z}\right)^2}.$$

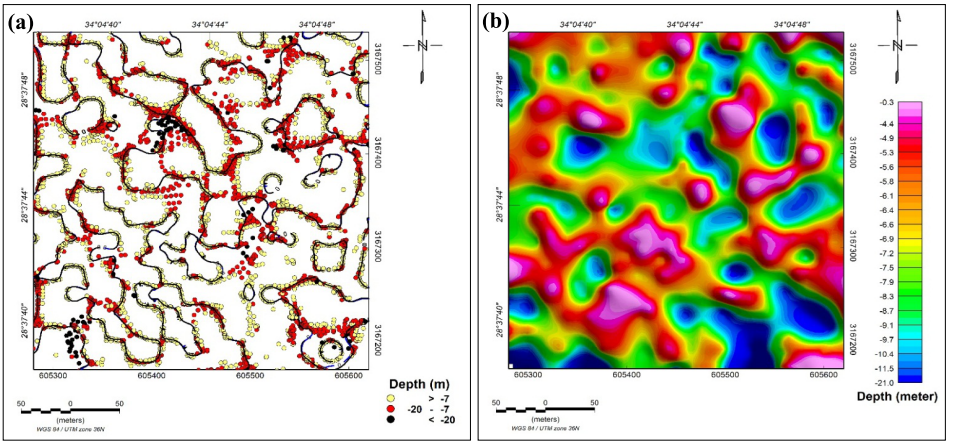

Fig. 8. Euler deconvolution solutions map of the study area (a) using SI = 0 obtained from RTP magnetic map, the solutions are superimposed on the zero-contours of the FVD and TDR maps; shaded-colour map of the calculated depths (b) using source parameter imaging (SPI) technique, Wadi Khosh El-Daba area, Southern Sinai, Egypt.

For the dipping contact, the maxima of K are located directly over the isolated contact edges and are independent of the magnetic inclination, declination, dip, strike and any remnant magnetization. The depth is estimated at the source edge from the reciprocal of the local wavenumber.

$$Depth_{(x=0)} = 1/K_{max}$$

where K_{max} is the peak value of the local of number K over the step source. The calculated depths using the source parameter imaging (SPI) technique are shown in Fig. 8b.

4.1.1. Interpretation of magnetic data

The interpretation of the magnetic maps is based on the fact that the intensity and size of the associated magnetic anomalies depend upon the depth, thickness, and size of the causative magnetic bodies. The basic intrusive, such as andesite dykes are associated with predominant positive magnetic anomalies, while, acidic intrusive, such as granites are associated with relatively negative anomalies.

The highest positive features in the RTP map (from −150 to 167 nT) are related mainly to the outcropped andesite dyke at the south-eastern part

of the study area, it appears in the form of linear feature trending in the NW–SE direction (Fig. 4b). This is followed by fairly positive anomalies of magnitude −260 to −150 nT magnetic features to the northeast, southwest, and southeast of the study area. They do not appear on the surface geology and may belong to shallow basic bodies beneath the monzogranites. They vary in shape and amplitude and are mostly directed to the NNW–SSE, NE–SW, and NW–SE. The lowest magnetic features (from −434 to −260) reflect local acidic rock composition at shallow depths (green to faint blue colour), and deep-seated acidic sources (deep blue colour) as shown in Fig. 4b. The contacts between negative and positive anomalies may be considered prospective areas for mineralization.

The residual map (Fig. 6a) exhibits the local anomalies which reflect the near-surface structures at about 19 m depth. It demonstrates the high-frequency anomalies originating from sources at shallow depths. The positive anomalies that appear in the RTP and residual maps and disappear in the regional map confirm that the causative sources of these anomalies are situated at the near-surface. The high positive magnetic anomalies observed along the RTP, residual, and regional maps in the same parts suggest that the causative sources of these anomalies have deep roots.

The regional map (Fig. 6b) reflects two broad positive anomalies related to the deep-seated changes in the structures of the basement rocks at about 37 m. The first anomaly with the highest positive values is related to the zones of relatively basic composition that trend in an NW–SE direction. These zones represent the source of the andesite dyke. These zones are followed in magnitude by the magnetic anomaly at the east of the study area which represents the root of the anomalies that appear in this zone in the RTP map. They are trending in an NE–SW direction. The low magnetic zones are located in the north-western part and the central part of the study area. They are separated by the NE–SW positive anomaly and represent deep seated acidic rocks.

The FVD map (Fig. 7a) displays shallow sources and structures, including dyke, faults, and contacts. These anomalies accompanied the outcropped andesite dyke and appear as a linear feature with high amplitude, the other anomalies spread through the study area with different shapes, sizes, and amplitudes indicating a relatively shallow depth for the underlying sources.

The zero-contour value on the TDR map defines subsurface lineaments (Fig. 7b). By comparing the FVD map with the TDR map, we found congruency between the zero-contour line of the two maps, confirming the locations of the magnetic bodies and their boundaries (faults/contacts) with the surroundings.

The Euler deconvolution (ED) approach was applied to the RTP grid by employing SI = 0, to calculate the lateral extent and depth of the magnetic contacts. The resulting ED map (Fig. 8a) demonstrates that the depths of the magnetic sources range from less than 7 m to 20 m. The source sites identified using ED are compatible with the zero contours of the FVD and TDR maps (Fig. 8a). The results of ED, FVD, and TDR confirm the horizontal locations and borders of the magnetic source bodies. On the other hand, the SPI depth estimates from the RTP grid (Fig. 8b) are close to those obtained from the Euler method and range from less than 3 m to about 21 m. These depths agree with that obtained from Euler depths relative to the structures.

The structural lineaments for the study area were deduced from the RTP, residual, regional, and FVD maps (Figs. 4b, 6a, 6b, and 7a). Statistical trend analysis was achieved to resolve the azimuths and lengths of the outlined interpreted lineaments. Rose diagrams were constructed for the interpreted structural lineaments (Fig. 9) to assist in defining the principal structural trends in the study area. The rose diagrams show that the NW–SE, NE–SW, and NNW–SSE trends in decreasing order of magnitude are related to near-surface structures in the study area. Meanwhile, the deepest trends are represented by the NW–SE, WNW–ESE, NNW–SSE, and E–W directions. The most important trends that affect the study area and govern the mineralization distribution are NW–SE, NE–SW, and NNW–SSE trends.

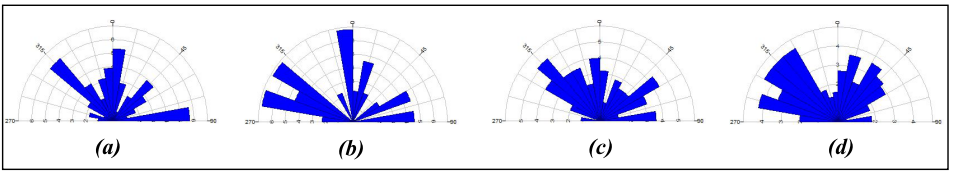

Fig. 9. Rose diagrams showing the main structural lineaments as deduced from RTP map (a), regional component map (b), residual component map (c), FVD map (d), Wadi Khosh El-Daba area, Southern Sinai, Egypt.

4.2. Self-potential (SP) data

The SP contour map of the study area (Fig. 10b) shows SP anomalous zones which are explained as mineralized zones controlled by structural features. Generally, in the SP measurements, the negatively stronger SP anomalies, the higher content of metallic mineralization. The positive response of the SP data is mainly associated with the resistant un-mineralized zones.

According to the SP values, the study area can be divided into three zones. The first zones have values less than −40 mV. These anomalies may arise from relatively stronger features of metallic mineralization where they are associated mainly with Wadi sediments and pegmatite vein. It is worth to mention that, *Bishr and Moselhy (2008)*, recorded radioactive mineralization in these two locations (Fig. 10b). The second zone included moderate to relatively weak SP anomalies ranging from −40 to −20 mV. These anomalies may be due to metallic mineralization associated with surface lineaments, such as faults (Fig. 10a), small streams, and contacts between andesite dyke and monzogranites. In additions, there are some weak SP anomalies are observed in the study area, with amplitude reaches to −20 millivolts. These anomalous zones may be related to surface geological, topographical, or de-

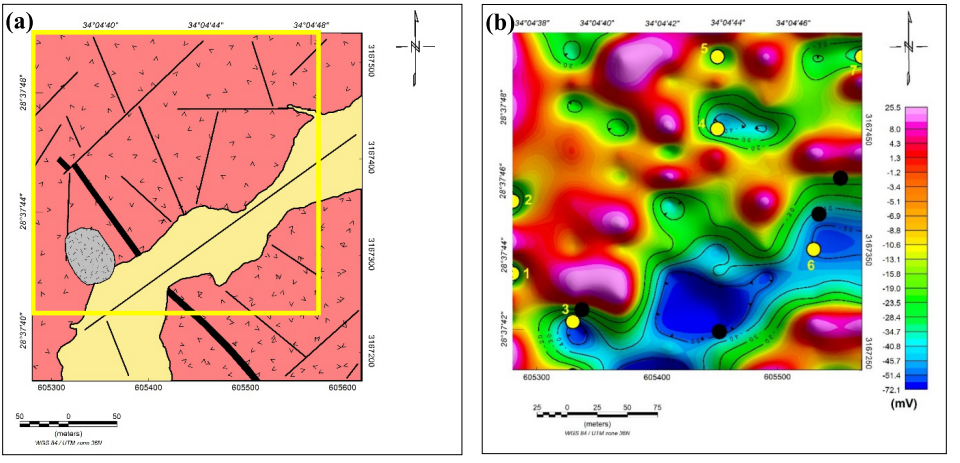

Fig. 10. The geologic map showing the selected area for the SP survey (yellow polygon) (a); self-potential shaded-colour map showing the locations of the alpha and gamma anomalies (b) according to *Bishr and Moselhi (2008)* (black circles), and the locations of the selected SP anomalies for the quantitative assessment (yellow circles), Wadi Khosh El-Daba area, Southern Sinai, Egypt.

positional features. The discontinuity of the anomalous zones along the fault trace shows that the mineralization zone is not related to the fault trace itself but may be due to its intersection with another element. They probably indicate subsurface structural features or mineralization occurrences.

Many trials for the quantitative interpretation of the SP survey data were carried out to obtain the causative location, depth, and dip for the observed SP anomalies. Babu and Rao method (*Babu and Rao, 1988*) is one of the most famous techniques that used in determining these parameters. It is a rapid graphical method for interpreting two-dimensional inclined sheets of finite depth extent. Using this method, the upper and lower edges of an inclined sheet of infinite strike extent can be located from the SP and anomaly curves $V(x)$ using a few characteristic points, including V_{max}, V_{min}, and V_0, (Fig. 11). The amplitude ratio ($R = V_{min}/V_{max}$) is shown to vary with θ, the dip of the sheet, making it possible to estimate θ.

From these characteristic features of $V(x)$, the sheet can be located easily using a simple geometrical construction (*Babu and Rao, 1988*). The following steps were carried out in this procedure:

i) Identification of the points $V_{max}, V_{min}, P_0, X_{max}, X_{min}$ and X_0, from the $V(x)$ curve (Fig. 11);

ii) Finding $R = V_{min}/V_{max}$, and reading the corresponding value of θ from the middle curve of Fig. 11a;

iii) Finding $V_1 = V_{max} + V_{min}$ and locating the points P_1 and P_2 at which $V(x) = V_1$;

iv) From P_1, the line P_1Q is drawn with $P_0P_1Q = \theta$;

v) From P_0, a perpendicular to the line P_1Q is dropped, which meet P_1Q at O, the centre of the sheet. The projection point O at the X-axis locates the origin ($X = 0$);

vi) A semicircle of diameter (X_{max}, to X_{min}) is drawn with its centre at P_0. This circle intersects the line P_1Q at A and B (the two edges of the sheet);

vii) Calculation the sheet parameter using the following equations:

$$h^2 = |x_0\, x_1|\,,$$

$$a = \sqrt{(x_{max}\,(\text{or } x_{min}) - x_0)^2 - h^2 \sec^2\theta}\,,$$

where h and a are the depth to the centre of the body and the half-width of the anomalous body, respectively.

In the present work, execution of this method gave reasonable results for only seven SP anomalies (No's l–7; "Fig. 10") whereas the characteristics of the other anomalies restrict the use of this method. The results of the application of this method show that the depths of the interpreted bodies causing the anomalies are shallow. The depths are ranging between 5.6 and 12.7 m from the surface, except anomaly No. 6, where it appears deeper than the others reaching 41 m. The inclinations of the interpreted body anomalies with the surface range between 18° and 33°. Finally, the half-width for the anomalous bodies are ranging between 5 m and 21 m (Table 1).

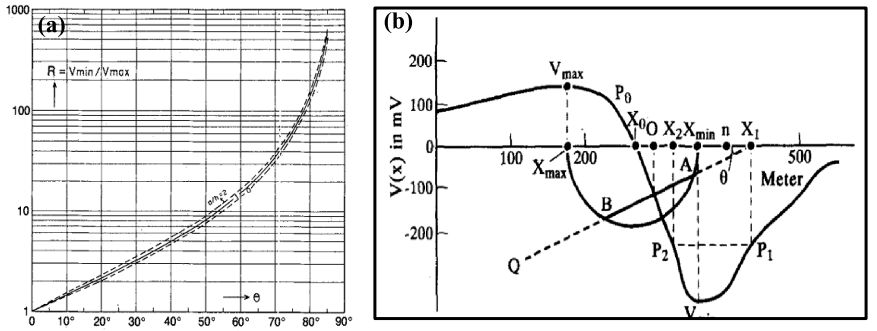

Fig. 11. Nomograms (a) showing the variation of R with θ; interpretation of the SP anomalies using the *Babu and Rao (1988)* method (b).

Table 1. Results of the quantitative interpretation for the selected SP anomalies, Wadi Khosh El-Daba area, Southern Sinai, Egypt.

profile No. (Fig. 4)	anomaly No. (Fig. 4)	calculated parameters			
		θ (°)	dipping direction	h (m)	a (m)
1	1	29.0	North	9.0	13.0
	2	33.0	South	12.7	14.0
2	3	30.0	North	7.0	16.0
5	4	50.0	South	7.7	5.3
	5	18.0	North	5.6	12.0
7	6	33.0	North	41.0	21.0
8	7	25.0	South	7.7	10.0

θ = dipping angle in degrees, h & a = depth to the centre of the body & half-width of the anomalous body in metres

To achieve the integration between the geophysical methods in this study with the collaboration of the previous study of *Bishr and Moselhy (2008)*, a compiled map is established to be includes SP, alpha, and gamma anomalies, which represent the surface and subsurface anomalies related to mineralization, all are superimposed on the ED solution and the zero-contours of the FVD map that refer to the locations and depths of faults and contacts of the magnetic bodies (Fig. 12a). The map shows that the radioactive and self-potential anomalies are structurally controlled, as they were distributed along the structural lineaments. They are distributed mainly along the NW–SE, NNW–SSE, and NE–SW structural trends and at the intersection of these trends. This map also shows similarities between the estimated depths from the self-potential and Euler's technique. Based on the radioactive and SP anomalies locations and the most affecting magnetic structural trends, four zones are considered promising for advanced exploration using the induced polarization (IP) method to delineate the exact distribution of the metallic subsurface mineralization (Fig. 12b).

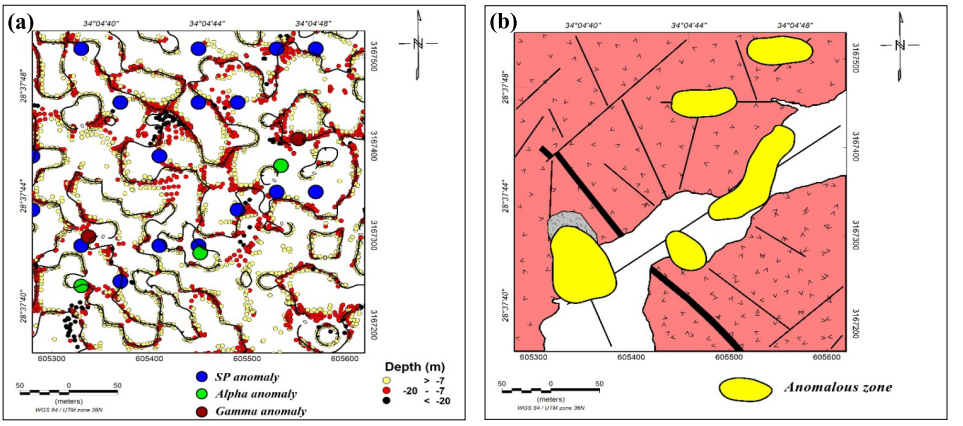

Fig. 12. SP, alpha, and gamma anomalies superimposed on the ED solution and the zero-contours of the FVD map (a); the geological map showing the locations of the anomalous zones (b), Wadi Khosh El-Daba area, Southern Sinai, Egypt.

5. Conclusions

The integration between the ground magnetic and self-potential methods enabled the determination of the main trends that control the distributions

of the mineralization in the study Wadi Khosh El-Daba area and the delineation of the mineralized zones, with obtaining important information about the lateral and vertical extensions for some selected SP anomalies in the area. In general, the results of the study can be concluded in the following points:

1. The magnetic survey data revealed that the estimated average depths for the shallow and deep magnetic sources, as calculated from the power spectrum curve, attain 19 m and 37 m, respectively.
2. From the application of analysis techniques such as FVD and TDR, it was found to enhance magnetic data, we found that the main structural elements affecting trends impacting the study area are oriented in the NW–SE, NE–SW, and NNW–SSE directions, with average depths reaching to 39 m and 21 m as deduced from using Euler and SPI techniques, respectively. Such structural elements govern the mineralization in the research area.
3. The SP measurements exhibit a wide range of amplitudes (−72 to +25.5 mV), with the highest negative values along the Wadi and the pegmatite vein. The distribution of these negative SP anomalies in the study area shows that there is a strong relation between their distribution and the contacts, fractures, and fault zones.
4. The calculation of the SP anomalies parameters revealed shallow depths to the centres of seven selected anomalies (except one anomaly located in the Wadi), ranging from 5.6 m to 41.0 m, while the half-widths of the anomalous bodies range from 5.3 m to 21 m. All the anomalies are moderately dipping have moderate dips to the South and the North directions.
5. There was a good agreement in surface spatial distribution between the main structural trends appearing in geology or obtained from magnetic data and the SP anomalies, which directly refer to the locations of hydrothermal activity zones.
6. The integration of the results obtained from using these techniques, in addition to the previous geological study, has shown the most appropriate zones for the development of further exploration in the area of investigation.

References

Arora T., Linde N., Revil A., Castermant J., 2007: Non-intrusive determination of the redox potential of landfill leachate plumes from self-potential data. J. Contam. Hydrol., **92**, 3-4. 274–292, doi: 10.1016/j.jconhyd.2007.01.018.

Assran A. S. M., Yousef M. H. M., Hassan N. F., Abd El Salam H. F., 2018: Self-potential, electromagnetic and gamma-ray spectrometric studies for Abu-Shihat area, North Eastern Desert, Egypt. Egypt. J. Appl. Geophys., **17**, 2, 1–12.

Babu H. V. R., Rao A. D., 1988: A rapid graphical method for the interpretation of the self-potential anomaly over a two-dimensional inclined sheet of finite depth extent. Geophysics, 53, 8, 1126–1128, doi: 10.1190/1.1442551.

Barbosa V., Silva J. B. C., Medeiros W. E., 1999: Stability analysis and improvement of structural index estimation in Euler deconvolution. Geophysics, **64**, 1, 48–60, doi: 10.1190/1.1444529.

Bentor Y. K., 1985: The crustal evolution of the Arabo-Nubian Massif with special reference to the Sinai Peninsula. Precambrian Res., **28**, 1, 1–74, doi: 10.1016/0301-9268(85)90074-9.

Bigalke J., Junge A., Zulauf G. 2004: Electronically conducting brittle-ductile shear zones in the crystalline basement of Rittsteig (Bohemian Massif, Germany): Evidence from self potential and hole-to-surface electrical measurements. Int. J. Earth Sci., **93**, 1, 44–51, doi: 10.1007/s00531-003-0364-5.

Bishr A. H. A., 2007: Factors controlling mineralizations of some shear zones in granites, South Sinai, Egypt. Ph.D. thesis, Geology Department, Faculty of Science, Zagazig University, Egypt.

Bishr A. H., Moselhi M., 2008: Using emanation coefficient and alpha-particle track detector for determination of subsurface anomalies and uranium minerals of Wadi Khosh El-Daba, South Sinai, Egypt. In: Proc. 9th Arab conference on the peaceful uses of atomic energy, Beirut, 13–16 Dec. 2008, 1–12.

Bogoch R., Zilberfrab A., 1979: Re-evaluation of the Wadi Remthi copper prospect. Geol. Surv. of Israel, Report no. M.P.B.K. 417/79.

Bølviken B., Logn O., 1975: An electrochemical model for element distribution around sulphide bodies. In: Elliot I. L., Fletcher W. K. (Eds.): Geochemical Exploration 1974: International Symposium Proceedings (Developments in economic geology). Elsevier, Amsterdam, 631–648.

Church B. N., 1984: Geology and self-potential survey of the Sylvester K gold-sulphide prospect (82E/2E). In: Geological fieldwork, 1983; A summary of field activities: British Colombia Ministry of Energy, Mines and resources paper 1984-1, pp. 7–14.

El-Aassy I. E., Hussein H. A., Zalata A. A., Abdel Meguid A. A., El-Metwally A. A., Ibrahim M. E., 1994: Radioactivity of Um Alawi environs, southern Sinai, Egypt. Egypt. J. Geol., 38, 1, 335–348.

El-Gammal S. A., 1986: Geology of the granitoid rocks of the northern western part of the basement rocks in Sinai, Egypt. Ph.D. thesis, Department of Geology, Faculty of Science, Al Azhar University, Egypt.

El-Ghawaby M. A., 1984: Image linear analytical approach to copper mineral exploration in south Sinai, Egypt. International workshop on remote sensing exploration, Trieste, Italy.

El-Ghawaby M. A., Hegazi A. M., Khalifa I. H., Arnous M. O., 2000: Tectonic and mineralization style of Saint Catherine Environs, South Sinai, Egypt. M.E.R.C. Ain Shams Univ., Earth Sci. Ser., **14**, 15–25.

Elkattan E. M., Adulhadi H. M., Rabie S. I., Hassanein H. I. E., 1996: Application of ground geophysical data to uranium mineralization in the El-Missikat area, central Eastern Desert, Egypt. J. Afr. Earth Sci., **22**, 1, 81–91, doi: 10.1016/0899-5362(95)00120-4.

El Shazly S. M., 1959: Recent investigations of Egyptian copper deposits. Symp. Appl. Geology in the Near East, Ankara 1955, Unesco, Cairo.

Fox R. W., 1830: On the electromagnetic properties of metalliferous veins in the mines of Cornwall. Philos. Trans. R. Soc. Lond., **120**, 399–414, doi: 10.1098/rstl.1830.0027.

Geosoft, 2014: Geosoft ver. 8.3; Geosoft mapping and processing system. Geosoft Inc., Toronto, Canada.

Gindy A. R., 1966: The origin of copper mineralization in central Sinai, U.A.R. 5th Arab Scientific Congress, Baghdad, Part 3, pp. 607–634.

Goldie M., 2002: Self-potentials associated with the Yanacocha high-sulfidation gold deposit in Peru. Geophysics, **67**, 3, 684–689, doi: 10.1190/1.1484511.

Hassen O. S., 1987: Geology and mineralization of El-Regeita area, Central south Sinai, Egypt. M.Sc. thesis, Fac. Sci., Suez Canal Univ., Ismailia, Egypt.

Horo D., Pal S. K., Singh S., Biswas A., 2023: New insights into the gold mineralization in the Babaikundi–Birgaon Axis, North Singhbhum Mobile Belt, Eastern Indian Shield using Magnetic, Very Low-Frequency Electromagnetic (VLF-EM), and self-potential data. Minerals, **13**, 10, 1289, doi: 10.3390/min13101289.

Hussein A. A. A., Ali M. M., El Ramly M. F., 1982: A proposed new classification of the granites of Egypt. J. Volcanol. Geotherm. Res., **14**, 1-2, 187–198, doi: 10.1016/0377-0273(82)90048-8.

Ibrahim M. E., 1991: Geology and radioactivity of Wadi Zaghra area, south central Sinai, Egypt. PH.D. thesis, Geology Department, Faculty of Science, Mansoura University, Egypt, 181 p.

Kearey P., Brooks M., 1991: An Introduction to Geophysical Exploration. Blackwell Scientific Publications, 2nd ed., London, Great Britain, 263 p.

Lowrie W., 2007: Fundamentals of Geophysics. 2nd edition, Cambridge University Press, 381 p.

Miller H. G., Singh V., 1994: Potential field tilt—a new concept for location of potential field sources. J. Appl. Geophys., **32**, 2-3, 213–217, doi: 10.1016/0926-9851(94)90022-1.

Mousa S. E. A., Elsayed R. A. M., Khalil A. F., Abd El-Nabi S. H., Yousef M. H. M., 2014: Delineating Cu-U mineralized zone in Wadi El-Regeita area, Southern Sinai-Egypt, using gamma-ray spectrometry and self-potential methods. EGS J. **13**, 1, 115–125.

Niazy E. A., Shalaby I. M., Abdel Rahim S. H., 1995: Wallrock alteration associated with the copper mineralization of Wadi El-Regeita, Southern Sinai, Egypt. Ann. Geol. Surv. Egypt, **20**, 433–450.

Nyquist J. E., Corry C. E., 2002: Self-potential: The ugly duckling of environmental geophysics. Lead. Edge, **21**, 5, 446–451, doi: 10.1190/1.1481251.

Parasnis D. S., 1997: Principles of Applied Geophysics. 5th ed., Chapman & Hall, London, ISBN 0-412-64080-5, 429 p.

Reid A. B., Allsop J. M., Granser H., Millett A. J., Somerton I. W., 1990: Magnetic interpretation in three dimensions using Euler deconvolution. Geophysics, **55**, 1, 80–91, doi: 10.1190/1.1442774.

Sato M., Mooney H. M., 1960: The electrochemical mechanism of sulphide self-potentials. Geophysics, **25**, 1, 226–249, doi: 10.1190/1.1438689.

Semenov A. S., 1974: Electrical prospecting with the natural electric field method. Nedra, Leningrad, 391 p. (in Russian).

Sharma P. V., 1997: Environmental and engineering geophysics. Cambridge University Press, 475 p.

Sultan A. S., Mansour S. A., Santos F. M., Helaly A. S., 2009: Geophysical exploration for gold and associated minerals, case study: Wadi El Beida area, South Eastern Desert, Egypt. J. Geophys. Eng., **6**, 4, 345–356, doi: 10.1088/1742-2132/6/4/002.

Telford W. M., Geldart L. P., Sheriff R. E., 1990: Applied Geophysics. 2nd ed., Cambridge University Press, 770 p.

Thurston J. B., Smith R. S., 1997: Automatic conversion of magnetic data to depth, dip, and susceptibility contrast using the SPI(TM) method. Geophysics, **62**, 3, 807–813, doi: 10.1190/1.1444190.

Yousef M. H. M., 2014: Laboratory and ground geophysical studies on the copper deposits and associated radioactive mineralizations, Wadi El-Regeita area, Southern Sinai, Egypt. Ph.D. thesis, Department of Geophysics, Faculty of Science, Ain Shams Univ., Egypt, 160 p.